Progress In Electromagnetics Research M, Vol. 16, 245–259, 2011

FLOATING INTERPOLATION STENCIL TOPOLOGY-BASED IE-FFT ALGORITHM

J. Yin, J. Hu, Z. Nie, X. Feng, and S. He

Department of Microwave Engineering
School of Electronic Engineering
University of Electronic Science and Technology of China (UESTC)
Chengdu 611731, China

Abstract—The integral equation fast Fourier transform (IE-FFT) is a fast algorithm for 3D electromagnetic scattering and radiation problems based on the interpolation of the Green's function. In this paper, a novel floating interpolation stencil topology is used to improve the IE-FFT algorithm. Compared to the traditional interpolation stencil topology, it can further reduce the storage and CPU time for the IE-FFT algorithm. The reduction is especially significant for volume integral equations. Furthermore, the accuracy of the algorithm is still good though the near-interaction element numbers are reduced. Finally, some numerical results including perfectly electric conductors, dielectric objects, composite conducting and dielectric objects are given to demonstrate the performance of the present method.

1. INTRODUCTION

The electromagnetic scattering and radiation problems that involve conducting, dielectric, composite conducting and dielectric objects find a wide applications in real world like the computation of radar cross section (RCS), electromagnetic compatibility (EMC) analysis, signal integrity in high speed interconnect in integrated circuit (IC) design, antenna analysis and optimal design. Most of these problems can be solved using one of these integral equation methods as surface integral equation (SIE), volume integral equation (VIE) and hybrid volume-surface integral equation (VSIE).

For perfectly electric conductor (PEC), only surface electric current need to solve, the SIE is a good choice for solving the

Received 31 October 2010, Accepted 27 January 2011, Scheduled 31 January 2011
Corresponding author: Jun Hu (hujun@uestc.edu.cn).

unknown current distributions [1]. In general, the combined field integral equation (CFIE) is used for closed objects and electric field integral equation (EFIE) is used for open structures. For arbitrary inhomogeneous dielectric objects, the VIE or VSIE is more preferred [2].

As well known, the memory and CPU time required for traditional method of moments (MoM) are both $O(N^2)$ for an iterative solver, where N is the number of unknowns. During the past several decades, many fast integral equation solvers have been developed to expedite the iterative solution of integral equation, such as conjugate gradient fast Fourier transform (CG-FFT) [3], multilevel fast multipole algorithm (MLFMA) [4, 5], adaptive integral method (AIM) [6, 7], precorrected fast Fourier transform (P-FFT) [8, 9], Green's function interpolation with fast Fourier transform (GIFFT) [10], integral equation fast Fourier transform (IE-FFT) [11, 12] and multilevel Green's function interpolation method (MLGFIM) [13]. The MLFMA has a low complexity of $O(N \log N)$ for arbitrary geometry shape, but it is a kennel dependent method and also has a low frequency breakdown problem. The CG-FFT is based on the circular convolution property of Green function, easy for implementation, however, it needs a uniform mesh which results in large modeling error for arbitrarily objects. The AIM, P-FFT, GIFFT and IE-FFT are FFT-based methods, require the complexity of $O(N^{1.5} \log N)$ for surface integral equation. In AIM and P-FFT, the matrix elements are calculated by mapping basis functions onto Dirac functions defined on the Cartesian grids with equal step cell, equivalent sources are need to represent the interactions between well separated elements. Unlike the AIM and P-FFT, the GIFFT and IE-FFT calculate matrix elements by mapping the Green's function onto interpolation functions defined on the Cartesian grids with equal step cell. The GIFFT approximates the Green's function over the interpolation grids as a sum of separable functions, is ideally suitable for solving array problems [10], while the IE-FFT simply interpolates the Green's function by Lagrange interpolation polynomials, calculates the interaction between nearby elements directly and expedites the interaction between far elements using FFT [11]. Different from the above methods, the MLGFIM uses multilevel discretization of the problem domain like MLFMA to realize the multilevel Green's function interpolation [13].

The heart of the IE-FFT algorithm is the interpolation of the Green's function. The interpolation of the Green's function is dependant of the choice of interpolation method and interpolation stencil. A novel interpolation method has been implemented to the IE-FFT algorithm to obtain a higher accuracy and lower computational

complexity and less memory costs in [14].

As well-known, a relative higher order interpolation technique and larger grid step are preferred for electrically large-scale problems, but it will result in large amount of near-interaction, especially for VIE, the memory and the CPU time required by the near-interaction dominate the total storage and CPU time. Thus, the CPU time and memory required in the IE-FFT algorithm are very expensive. To overcome these problems, a floating interpolation stencil topology used in AIM [6], P-FFT [15] is firstly applied into the IE-FFT method here to reduce the cost of near-interaction. In this case, the Green functions are projected by Lagrange interpolation polynomials associated with the interpolation Cartesian cell dependent on the location of the considered basis function support. The Cartesian cell assigned to a basis is a cell whose center is nearest to the center of the support of the original basis function. Because the new stencil makes the basis functions closer to the center of the interpolation Cartesian cells, the interpolation accuracy is improved especially for higher order interpolation case. In the other hand, the total cost of near-interaction is reduced greatly by avoiding direct storage and computation of plenty of matrix entries in traditional IE-FFT.

The outline of this paper is as follows. We describe how the floating interpolation stencil topology reduces the memory requirements and computational complexity in Section 2. In Section 3, we present some numerical results to demonstrate the efficiency and accuracy of the floating interpolation stencil topology. Finally, the summary of this paper is given.

2. IE-FFT ALGORITHM

The basic idea of the IE-FFT algorithm is to interpolate the Green's function, separates the interaction into near and far interactions, and calculates the near-interaction elements directly and expedites the far-interaction using the FFT.

2.1. Traditional IE-FFT

To demonstrate clearly the basic idea of the IE-FFT, here we first consider the EFIE solution of PEC scattering, in general, the entry of EFIE matrix can be expressed by the following general formula

$$Z_{mn} = \int_{\Delta m} \int_{\Delta n} \tau_m \left(\mathbf{r}\right) G\left(\mathbf{r}, \mathbf{r}'\right) \tau_n \left(\mathbf{r}'\right) dr' dr \tag{1}$$

where $\tau_m \left(\mathbf{r}\right)$ denotes the functions related to the mth testing function, such as the testing function or the gradient of testing function. $G\left(\mathbf{r}, \mathbf{r}'\right)$

is the free space Green's function.

To apply the IE-FFT algorithm, a bounding rectangular box is constructed to enclose the scatter, then the bounding box is partitioned uniformly into Cartesian cells which will be used to interpolate the Green's function as show in Fig. 1.

$$G\left(\mathbf{r},\mathbf{r}'\right)=\sum_{l=0}^{M^3}\sum_{l'=0}^{M^3}\beta_l^M\left(\mathbf{r}\right)\mathbf{G}_{ll'}\beta_{l'}^M\left(\mathbf{r}'\right) \tag{2}$$

where M is the interpolation order, the $\mathbf{G}_{ll'}$ denotes the Green's functions between the Cartesian grids and $\beta_l^M(\mathbf{r})$ is the Lagrange interpolation basis functions, denoted as,

$$\beta_l^M\left(\mathbf{r}\right)=\beta_i^M\left(x\right)\cdot\beta_j^M\left(y\right)\cdot\beta_k^M\left(z\right) \tag{3}$$

where

$$\beta_i^M\left(x\right)=\prod_{i'=0,i'\neq i}^{M}\left(\frac{x-x_{i'}}{x_i-x_{i'}}\right) \tag{4}$$

Substituting (2) into (1), the matrix entry can be written as

$$\begin{aligned}\mathrm{Z}_{mn}^{IE-FFT} &= \sum_{l=0}^{M^3}\sum_{l'=0}^{M^3}\left(\int_{\Delta m}\tau_m\left(\mathbf{r}\right)\beta_l^M\left(\mathbf{r}\right)d\mathbf{r}\right)\cdot\mathbf{G}_{ll'}\\ &\quad\cdot\left(\int_{\Delta n}\tau_n\left(\mathbf{r}'\right)\beta_{l'}^M\left(\mathbf{r}'\right)d\mathbf{r}'\right)=\mathbf{\Pi}_{ml}\cdot\mathbf{G}_{ll'}\cdot\mathbf{\Pi}_{l'n}^T\end{aligned} \tag{5}$$

where $\mathbf{\Pi}_{ml}$ denotes projection matrix. Since the near-interaction elements will face with the singularity of Green function if calculated by interpolation technique, the near-interaction elements should be corrected by the method of moment (MoM) in matrix form as

$$\mathbf{Z}^{near}=\mathbf{Z}_{MoM}^{near}-\mathbf{Z}_{IE-FFT}^{near} \tag{6}$$

For the Green's matrix G is a Toeplitz matrix, so FFT can be used to expedite the matrix-vector multiplication as

$$\begin{aligned}\mathbf{Z}\cdot\mathbf{I} &= \left(\mathbf{Z}_{MoM}^{near}-\mathbf{Z}_{IE-FFT}^{near}\right)\cdot\mathbf{I}+\mathbf{Z}_{MoM}^{far}\cdot\mathbf{I}+\mathbf{Z}_{IE-FFT}^{near}\cdot\mathbf{I}\\ &\approx \mathbf{Z}^{near}\cdot\mathbf{I}+\mathbf{Z}_{IE-FFT}\cdot\mathbf{I}\\ &= \mathbf{Z}^{near}\cdot\mathbf{I}+\mathbf{\Pi}\cdot F^{-1}\left\{F\left\{\mathbf{G}\right\}\cdot F\left\{\mathbf{\Pi}_T\cdot\mathbf{I}\right\}\right\}\end{aligned} \tag{7}$$

where F and F^{-1} stand for FFT and inverse FFT respectively. $\mathbf{\Pi}$ and $\mathbf{\Pi}^T$ are the projection matrices.

Based on Eq. (2), we can easily compute the gradient of the Green's function by applying the gradient operator on the Lagrange

polynomials. So the gradient of the Green's function can be interpolated as

$$\nabla G\left(\mathbf{r},\mathbf{r}'\right)=\sum_{l=0}^{M^3}\sum_{l'=0}^{M^3}\nabla\beta_l^M\left(\mathbf{r}\right)\mathbf{G}_{ll'}\beta_{l'}^M\left(\mathbf{r}'\right) \tag{8}$$

For conducting objects, the following function sets will be required to realize a CFIE solution,

$$\tau_n\in\left\{\mathbf{f}_n,\nabla\cdot\mathbf{f}_n,\hat{n}\times\mathbf{f}_n,\nabla\beta\times\mathbf{f}_n\right\} \tag{9}$$

where $\mathbf{f}_n$ is the curvilinear Rao-Wilton-Glisson (RWG) basis function [16–18].

For dielectric objects solved by volume integral equation, similarly we have

$$\tau_n\in\left\{\kappa\mathbf{f}_n^V,\nabla\cdot\left(\kappa\mathbf{f}_n^V\right)\right\} \tag{10}$$

where κ is the contrast ratio, $\mathbf{f}_n^V$ is the Schaubert-Wilton-Glisson (SWG) basis function [19].

And for composite PEC and dielectric objects by volume and surface integral equation, we also have

$$\tau_n\in\left\{\begin{array}{l}\mathbf{f}_n^S,\kappa\mathbf{f}_n^V,\nabla\cdot\mathbf{f}_n^S,\nabla\cdot\left(\kappa\mathbf{f}_n^V\right),\\ \hat{n}\times\mathbf{f}_n^S,\nabla\beta\times\mathbf{f}_n^S,\nabla\beta\times\mathbf{f}_n^V\end{array}\right\}. \tag{11}$$

where $\mathbf{f}_n^S$ is the RWG basis function [16].

Obviously, only the interpolation of scalar Green function is required in the above all IE cases, so the implementation of the IE-FFT into the CFIE, VIE, VSIE is similar to the one into the SIE and also easy to do.

2.2. The Floating Interpolation Stencil Topology

In the traditional IE-FFT implementation, as show in Fig. 1, first, a bounding rectangular box is constructed to enclose the PEC disk, then the bounding box is partitioned uniformly into Cartesian cells which will be used to interpolate the Green's function. This interpolation stencil will generate unnecessary near-interaction cost, as shown in later.

For example, in Fig. 1, the bounding box is partitioned into 3×3 Cartesian cells, basis function A (BF_A) uses Cartesian cell 1 to interpolate the Green's function and BF_B uses Cartesian cell 2 to interpolate the Green's function, the distance between BF_A and BF_B in Fig. 1 is far enough to satisfy the well-separated threshold distance (e.g., 0.2λ, where λ is the free space wavelength).

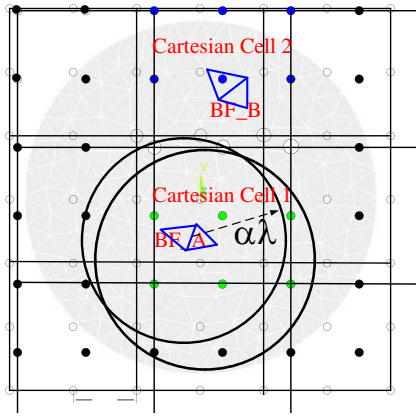

Figure 1. Traditional IE-FFT Cartesian cells, the three bigger (white) grid nodes are shared grid nodes. PEC disk (shadow) is enclosed.

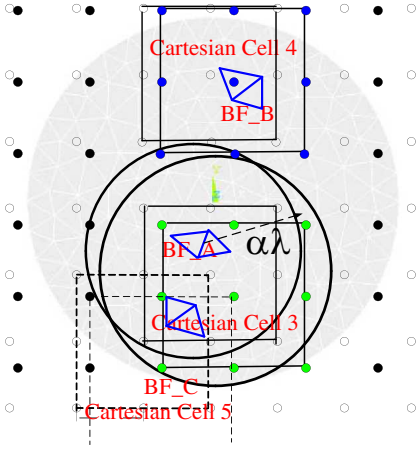

Figure 2. Cartesian cells of IE-FFT with floating interpolation stencil topology.

However, the interpolation Cartesian cells (Cartesian cell 1 and Cartesian cell 2) where they reside shared grid nodes, and the Green's function has singularities ($G_{ll'} = \infty$, when $l = l'$). So the interaction between them can be only computed by the MoM directly though the distance between BF_A and BF_B satisfies the well-separated condition. Obviously, this will leads to store and compute a lot of unnecessary near-interaction elements in the traditional interpolation stencil.

To overcome this problem, the floating interpolation stencil topology [6, 15] is introduced here. The floating interpolation stencil is constructed as follows: first, generate the same grid nodes as the traditional IE-FFT, and then set each inner grid node as the center of an interpolation Cartesian cell. In this meaning, the Cartesian cells are overlapped with each other. For this stencil, one basis function may reside in several interpolation Cartesian cells, here we define that the basis function belongs to the interpolation Cartesian cell whose center is nearest to the basis function. For example, BF_C reside in Cartesian cell 3 and Cartesian cell 5, but the center of Cartesian cell 5 is much closer to BF_C than Cartesian cell 3, so BF_C belongs to Cartesian cell 5 as shown in Fig. 2.

In Fig. 2, the grid nodes are the same as Fig. 1. When using the floating interpolation stencil topology, BF_A use Cartesian cell 3 to interpolate the Green's function and BF_B use Cartesian cell 4 to

interpolate the Green's function. It is shown that Cartesian cell 3 and Cartesian cell 4 share no grid nodes, so their interactions needn't to be corrected. Hence, the near-interaction cost is reduced greatly by applying the floating interpolation stencil topology.

3. NUMERICAL RESULTS

In this section, we present some numerical examples to demonstrate the accuracy of the floating interpolation stencil topology and the comprehensive efficiency and accuracy of the present IE-FFT algorithm. Different from traditional IE-FFT, here $\beta_l^M(\mathbf{r})$ is chosen to be Gaussian interpolation basis functions [14] in order to assure a good precision of interpolation of Green functions. All the problems are solved on a 64 bit Dell workstation.

For sake of simplicity, one variable free space Green's function $g(x) = e^{ikx}/4\pi x$ is considered here to demonstrate the accuracy of the floating interpolation stencil topology. We assume that the source point is located at the origin point ($x = 0$), the observation points are distributed in the interval between $0.2\lambda \sim 1.1\lambda$, where λ is the free space wavelength. The Green's function $g(x)$ between the source point and observation point is interpolated by the Green's function $g(x_i)$ at grid nodes, where x_i are the grid nodes. Here, the interpolation order is set to be 3.

When using traditional interpolation stencil, the interpolation domain is uniformly partitioned into 3 Cartesian cells as shown in Fig. 3(a). Obviously, the Green's function between the field point (red square) and observation point is interpolated by using Cartesian cell 2.

However, in Fig. 3(b), the interpolation domain is partitioned into 7 overlapped Cartesian cells when using floating interpolation stencil topology. The field point (red square) is nearest to the center of Cartesian cell 5, thus it belongs to Cartesian cell 5. Fig. 3 shows that the floating interpolation stencil topology makes the field point closer to the center of its interpolation Cartesian cell. Hence, the interpolation accuracy is more accurate than the traditional interpolation stencil topology.

Figure 4 shows the relative error of the interpolated Green's function versus the distance between the source and observation point, i.e., x ($y = z = 0$), for different interpolation stencil. Fig. 5 shows the root mean square (RMS) error versus the grid step for different interpolation stencil and Fig. 6 shows the RMS error versus the interpolation order for different interpolation stencil. Obviously, the floating stencil has a higher accuracy than the traditional interpolation stencil.

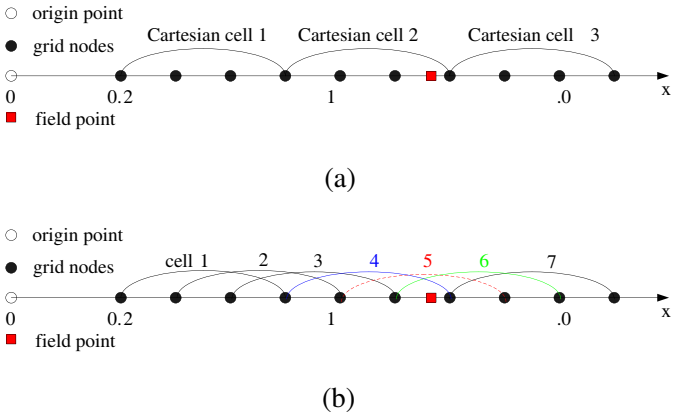

Figure 3. The interpolation stencil to calculate the Green's function. (a) Traditional interpolation stencil, (b) floating interpolation stencil.

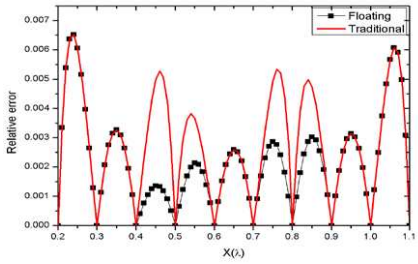

Figure 4. Relative error of the interpolated Green's function versus the distance between source and observation point for different interpolation stencil.

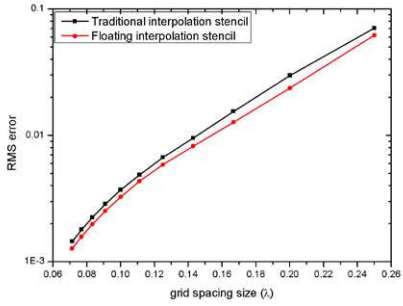

Figure 5. The RMS error versus the grid spacing size for different interpolation stencil.

To further demonstrate the accuracy of IE-FFT algorithm with floating interpolation stencil, a PEC sphere with a radius of 1m is investigated with different mesh density. The frequency of the incident wave is 300 MHz. The interpolation order is 3. The RMS errors of IE-FFT with floating interpolation stencil and IE-FFT with traditional interpolation stencil are summarized in Table 1. It shows that the RMS errors of IE-FFT with floating interpolation stencil are lower than that of IE-FFT with traditional interpolation stencil.

In the following, some typical scattering and radiation cases are

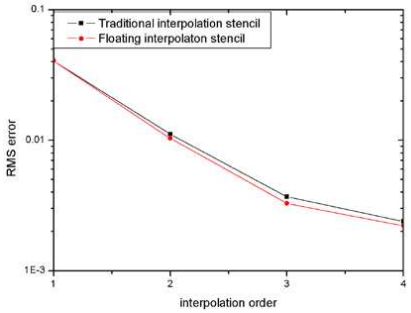

Figure 6. The RMS error versus interpolation order for different interpolation stencil.

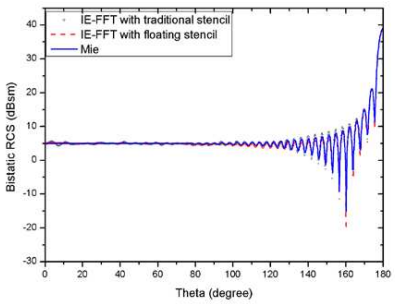

Figure 7. HH polarized bistatic RCS of a PEC sphere at 2.4 GHz.

Table 1. The RMS error of different number of unknowns for a PEC sphere $f = 300$ MHz.

Mesh size (m)	Number of unknowns	RMS error for IE-FFT with floating stencil (dBsm)	RMS error for traditional IE-FFT (dBsm)
1/8	2424	0.13	0.24
1/16	10077	0.10	0.19
1/32	41265	0.04	0.10

solved by the present method. Except mentioned specially, the grid step $\Delta = 0.1\lambda$, the near-interaction threshold $d_{near} = 0.2\lambda$, and the 2nd order interpolation is used, where λ is the free space wavelength.

3.1. PEC Objects

To demonstrate the efficiency and accuracy of the floating interpolation stencil topology for PEC objects, a PEC sphere with a radius of 1 m is considered. The HH polarized bistatic RCS is calculated at 2.4 GHz with 101,328 unknowns. The RCS results show good agreement with Mie series solution in Fig. 7. The RMS error is 0.04 dBsm for IE-FFT with floating interpolation stencil and 0.05 dBsm for traditional IE-FFT respectively.

The memory requirement is 817.24 MB for IE-FFT with floating stencil and 990.41 MB for IE-FFT with traditional stencil. The CPU time for correction is almost 5 minutes, 20 minutes for IE-FFT with floating stencil, traditional stencil respectively. And the CPU time per

iteration is 510.67 seconds, 513.73 seconds for IE-FFT with floating stencil, traditional stencil respectively.

To demonstrate the ability of the present method for real-life applications, scattering from a complicated PEC aircraft model is investigated. The bistatic RCS in VV polarization is calculated at 1GHz with the plane wave incident from the nose (theta = 90°, phi = 0°). The length is 50 wavelength, the number of unknowns is 704,070. The result is shown in Fig. 8. A good agreement with the results by our MLFMA code [20] is also achieved by the present IE-FFT.

The memory requirement is 4.825 GB for IE-FFT with floating stencil. The CPU time for correction is almost 50 minutes for IE-FFT with floating stencil. It takes 137 steps to finish the CG iteration with no pre-conditioner.

To demonstrate the ability of the present method for large scale problem, the bistatic RCS of a PEC sphere with radius of 1 m is computed using an IE-FFT accelerated CFIE solver with the floating interpolation stencil. The frequency of excitation is 7.5 GHz, $N = 1,015,230$ and the CFIE factor $\alpha = 0.5$. In this simulation, the grid step size $\Delta = 0.15\lambda$, $M = 3$. The calculation requires 10.876 GB storage and 67.8 hours CPU time. The RMS error relative to Mie series solution is only 0.032, so the accuracy of the present method is very good, even for the large scale problems.

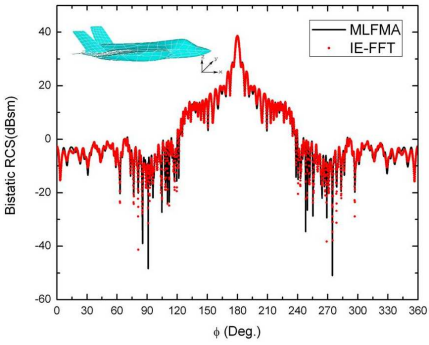

Figure 8. The bistatic RCS of a complicated aircraft model at 1 GHz (VV polarization).

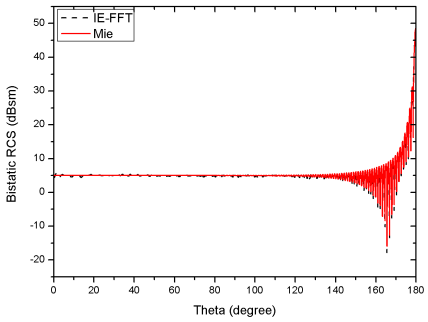

Figure 9. The HH polarized bistatic RCS of a 50λ PEC sphere.

3.2. Dielectric Objects

Here, we apply the present method with VIE to solve the dielectric problem. First, a lossy dielectric shell is considered. The inner radius of the dielectric shell is 1.5 m and the outer radius of the dielectric shell is 1.6 m. The dielectric permittivity is $1.5 + 0.5i$, the incidence frequency is 300 MHz. The shell is discretized into 6,500 tetrahedrons with 15,168 unknowns, solved by using an IE-FFT accelerated VIE solver. The bistatic RCS is plotted is Fig. 10.

The memory requirement is 74.04 MB, 178.07 MB for IE-FFT with floating interpolation stencil, traditional interpolation stencil respectively. The CPU time for correction is almost 4 minutes, 20 minutes for floating interpolation stencil, traditional stencil respectively. And the CPU time per iteration is 2.98 seconds, 7.18 seconds for IE-FFT with floating interpolation stencil, traditional one respectively.

The second example is a nine elements dipole array beside a dielectric cube. The geometry of the problem is shown in Fig. 11. The edge length of the cube is of 1λ, where λ is the free space wavelength. The dielectric permittivity is of $2.0 + i1.0$. A 9-element uniform dipole array with 0.375λ inner-element spacing is set on the z-axis beside the cube. The array operates at 300 MHz. The radiated field of the dipole array is shown in Fig. 12, compared with the AIM solution [21]. The cube is solved with 25,954 unknowns by using an IE-FFT accelerated VIE solver with floating interpolation stencil.

The memory requirement is 320.37 MB and the CPU time for correction is almost 35 minutes for IE-FFT. A good agreement between the IE-FFT and AIM is shown in Fig. 12. The effect of dielectric cube on the radiation pattern of dipole array is very distinct.

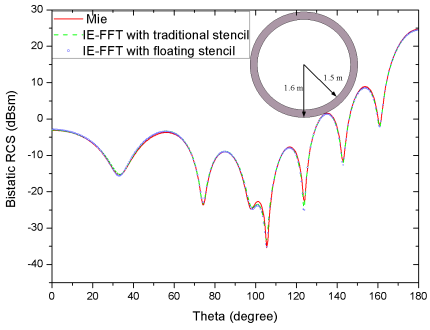

Figure 10. Bistatic RCS of a spherical dielectric shell.

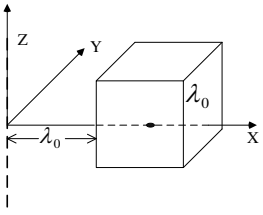

Figure 11. Nine element dipole array beside a dielectric cube.

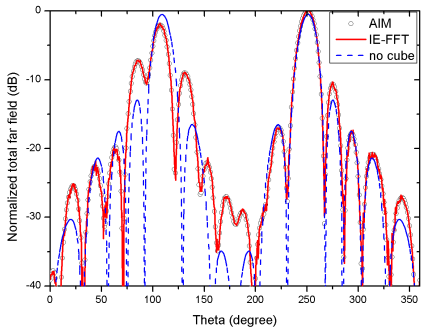

Figure 12. Normalized total far field of nine element dipole array beside a dielectric cube.

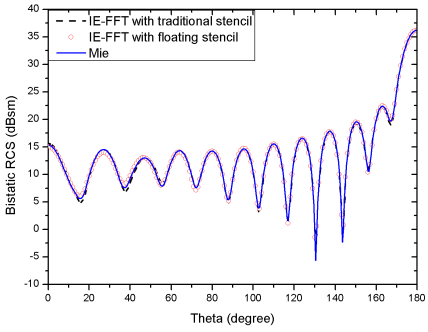

Figure 13. Bistatic RCS of a coated sphere. The radius of sphere is 2.0 m, the thickness is 0.1 m.

3.3. Composite Conducting and Dielectric Objects

The final example is a coated conducting sphere, the core sphere has a radius of 2.0 m and the thickness of the coating layer is 0.1 m. The relative permittivity of the coating layer is 2. The Bistatic RCS is calculated at 300 MHz with 124,979 total unknowns using an IE-FFT accelerated VSIE solver. The RCS results show good agreement with the Mie series solution in Fig. 13.

For this case, the memory requirement is 2.056 GB, 5.748 GB for IE-FFT with floating interpolation stencil, traditional interpolation stencil respectively. The CPU time for correction is almost 149 minutes, 588 minutes for IE-FFT with floating interpolation stencil and traditional one, respectively. And the CPU time per iteration is 47.78 seconds for IE-FFT with floating stencil and 67.75 seconds for traditional stencil.

The comparison of performance of IE-FFT with floating interpolation stencil topology with traditional one is tabulated finally. As shown in Table 2, for surface integral equations, the memory needed to store the matrix related into Green functions and the CPU time to calculate the FFT dominate the total memory and CPU time, so the improvement is not so remarkable. But for volume integral equations, the memory and the CPU time required for the near-interaction dominate the total memory and CPU time, thus the improvement is very significant.

Table 2. Performance of the floating interpolation stencil topology-based IE-FFT algorithm with $M = 2$.

	Number of unknowns	CPU time per iteration (s)		CPU time for correction matrix (minutes)		Total memory	
		traditional	floating stencil	traditional	floating stencil	traditional	floating stencil
PEC Sphere (SIE)	101,328	513.73	510.67	20	5	990.41 MB	817.24 MB
spherical shell (VIE)	15,168	7.18	2.98	20	4	178.07 MB	74.04 MB
coated sphere (VSIE)	124,979	67.75	47.78	588	149	5.748 GB	2.056 GB

4. CONCLUSION

In this paper, the IE-FFT algorithm based on the floating interpolation stencil topology is developed for enhancing the efficiency of solution of 3D scattering and radiation problems. All the matrix entries calculated by IE-FFT satisfy the well-separated distance threshold, those elements reduced by using the floating interpolation stencil can be computed by the IE-FFT accurately, which cannot be applied in traditional one due to the singularity of the Green's function. So the proposed method reduces greatly the CPU time and memory requirements of the IE-FFT algorithm while the accuracy of the algorithm is still good. The numerical result shows that the reduction is significant, especially for the case of volume integral equations.

ACKNOWLEDGMENT

This work is supported partly by NSFC (No. 60971032), the Programme of Introducing Talents of Discipline to Universities under Grant b07046, research funding under G02010201PJ09DZ0212.

REFERENCES

1. Mautz, J. R. and R. F. Harrington, "*H*-field, *E*-field and combined-field solution for conducting bodies of revolution," *AEU*, Vol. 32, No. 4, 157–164, 1978.
2. Lu, C. C. and W. C. Chew, "A coupled surface-volume integral equation approach for the calculation of electromagnetic scattering from composite metallic and material targets," *IEEE Trans. Antennas Propagat.*, Vol. 48, No. 12, 1866–1868, Dec. 2000.
3. Sarkar, T. K., E. Arvas, and S. M. Rao, "Application of FFT and the conjugate gradient method for the solution of electromagnetic radiation from electrically large and small conducting bodies," *IEEE Trans. Antennas Propagat.*, Vol. 34, 635–640, May 1986.
4. Song, J. M. and W. C. Chew, "Multilevel fast multipole algorithm for solving combined field integral equation of electromagnetic scattering," *Microw. Opt. Tech. Lett.*, Vol. 10, No. 1, 14–19, Sep. 1995.
5. Song, J. M., C. C. Lu, and W. C. Chew, "Multilevel fast multipole algorithm for electromagnetic scattering by large complex objects," *IEEE Trans. Antennas Propagat.*, Vol. 45, 1488–1493, Oct. 1997.
6. Bleszynski, E., M. Bleszynski, and T. Jaroszewicz, "AIM: Adaptive integral method for solving large-scale electromagnetic scattering and radiation problems," *Radio Science,* Vol. 31, No. 5, 1225–1251, 1996.
7. Bindiganavale, S. S., J. L. Volakis, and H. Anastassiu, "Scattering from planar structures containing small features using the adaptive integral method (AIM)," *IEEE Trans. Antennas Propagat.*, Vol. 46, 1867–1878, Dec. 1998.
8. Phillips, J. R. and J. K. White, "A Precorrected-FFT method for electrostatic analysis of complicated 3-D structures," *IEEE Trans. Computer-aided Design of Integrated Circuit and Systems*, Vol. 16, 1059–1072, Oct. 1997.
9. Nie, X., L.-W. Li, N. Yuan, and Y. T. Soon, "Pre-corrected FFT algorithm for solving combined field integral equations in electromagnetic scattering," *Journal of Electromagnetic Waves and Applications,* Vol. 16, No. 8, 1171–1187, 2002.
10. Fasenfest, B. J., F. Capolino, D. R. Wilton, D. R. Jackson, and N. J. Champagne, "A fast MoM solution for large arrays: Green's function interpolation with FFT," *IEEE Antennas and Wireless Propagation Letters,* Vol. 3, 161–164, Dec. 2004.
11. Seo, S. M. and J. F. Lee, "A fast IE-FFT algorithm for solving

PEC scattering problems," *IEEE Trans. Magn.*, Vol. 41, 1476–1479, May 2005.

12. Ozdemir, N. A. and J. F. Lee, "IE-FFT algorithm for a nonconformal volume integral equation for electromagnetic scattering from dielectric objects," *IEEE Trans. Magn.,* Vol. 44, 1398–1401, Jun. 2008.
13. Li, L., H. G. Wang, and C. H. Chan, "An improved multilevel Green's function interpolation method with adaptive phase compensation," *IEEE Trans. Antennas Propagat.*, Vol. 56, No. 5, 1381–1393, May 2008.
14. Lai, B., X. An, et al., "A novel Gaussian interpolation formula-based IE-FFT algorithm for solving EM scattering problems," *Microwave and Optical Technology Letters,* Vol. 51, No. 09, 2233–2236, Sep. 2009.
15. Chen, Z. K., S. L. Chai, H. Yang, and J. J. Mao, "Precorrected-FFT method for EM scattering from composite metallic-dielectric objects," *Chinese Sci. Bull.*, Vol. 55, 656–663, 2010.
16. Rao, S. M., D. R. Wilton, and A. W. Glisson, "Electromagnetic scattering by surfaces of arbitrary shape," *IEEE Trans. Antennas Propagat.,* Vol. 30, No. 5, 409–418, May 1982.
17. Graglia, R. D., D. R. Wilton, and A. F. Peterson, "High order interpolatory vector bases for computational electromagnetics," *IEEE Trans. Antennas Propagat.*, Vol. 45, No. 3, 329–342, Mar. 1997.
18. Hu, J., Z. Nie, and X. Gong, "Solving electromagnetic scattering and radiation by FMM with curvilinear RWG basis," *Chinese Journal of Electronics*, Vol. 12, No. 3, 457–460, 2003.
19. Schaubert, D. H., D. R. Wilton, and A. W. Glisson, "A tetrahedral modeling method for electromagnetic scattering by arbitrarily shaped inhomogeneous dielectric bodies," *IEEE Trans. Antennas Propagat.*, Vol. 32, No. 1, 77–85, Jan. 1984.
20. Hu, J. and Z. Nie, "Improved electric field integral equation (IEFIE) for analysis of scattering from 3-D conducting structures," *IEEE Trans. Electromagn. Compat.*, Vol. 49, No. 3, 644–648, Aug. 2007.
21. Guo, J.-L., J.-Y. Li, and Q.-Z. Liu, "Analysis of arbitrarily shaped dielectric radomes using adaptive integral method based on volume integral equation," *IEEE Trans. Antennas Propagat.*, Vol. 54, No. 7, 1910–1916, Jul. 2006.